Noncontact 3D measurement method on hole-structure precision inspection*

SHI Hao-tian (施皓天)[1], **WU Di** (伍狄)[1], **PANG Cheng-kai** (庞程凯)[1], **HUANG Hai-yan** (黄海燕)[1], **ZHANG Xuan** (张璇)[2], **XU Yan** (徐焱)[2], **CHEN Xiu-liang** (陈修亮)[1]**, and **WU Guang** (吴光)[1]

1. State Key Laboratory of Precision Spectroscopy, East China Normal University, Shanghai 200241, China

2. AECC Commercial Aircraft Engine Co., Ltd., Shanghai 200241, China

(Received 19 May 2020; Revised 22 July 2020)

In order to implement 3D point cloud scanning of small hole structure, which could not be contacted or damaged, we propose a noncontact 3D measuring method. The system contains a laser triangulation displacement sensor, a Michelson interferometer system and a coordinate measuring machine, with the advantages of non-invasive scanning, fast measurement speed and high precision. Focusing on reconstructing 3D point cloud data, random sample consensus is used to separate surface data and hole data respectively from the raw dataset. Least square optimization determines the function of the cylinder, as well as hole diameter and inclined angle between the hole and the surface. In the experiment scanning a round hole, the estimated result has diameter error and angle error within 30 μm and 0.2°, respectively. Results manifest the effectiveness and feasibility of this system and express practicality in manufacturing industry.

Document code: A **Article ID:** 1673-1905(2021)04-0231-5

DOI https://doi.org/10.1007/s11801-021-0084-8

Small holes were widely applied in industrial manufacturing, such as ink-jet printer nozzles, the spray holes of diesel and cooling vents for gas turbine blade. The size and orientation of the holes affect the efficiency and exhaust emission of the diesel engines, the cooling performance of the turbine blade. Therefore, measurement of the holes plays a significant role in industrial manufacturing[1-4]. In an early approach, a plug gauge of the proper diameter is inserted in the hole. The size of the hole is between the tight fit plug and loose fit plug. In the turbine blade, air gauging provides a more efficient measure of holes. Two jets of air flow towards the wall of the hole in opposite direction. The diameter of the hole was calculated by measuring the back pressure exerted on the air flow. This method is quite efficient, but it only works well in a very short range of holes, and it cannot find out the detail of the defects. The size of the holes can also be measured by a coordinate measuring machine with a contact trigger probe. However, as the contact was required to make a measurement in a coordinate measuring machine (CMM), which can result in wear and breakage, it cannot be applied in the surface of ultra-precision and highly polished alloy and soft fabric. Limited to the size of the contact probe and the measurement speed, the normal CMM is rarely used to measure holes with diameter less than 1 mm. To measure tiny structures, researchers developed much smaller probes. Peiner and Doering presented a piezoresistive cantilever sensor in inspecting form and roughness inside nozzle holes of 100—200 μm in diameter. The sensor had an average deviation of ±2 nm scanning at a speed of 100 μm/s[5].

With the development of optical measurement technology, optical measuring system was employed to measure the fine structure of small holes. Confocal and low coherence distance scanning device were used to measure hole geometry, which can provide micro meter level accuracy and precision[6-8]. A NIST fiber probe, which is made from a glass fiber with a ball formed on the end, was used instead of the conventional contact probe. This probe enables the inspection of micro holes with diameter of a hundred micrometer. As the structure and measurement process of these optical measuring system, the measurement speed of these technology is quite slow, and cannot be applied in in-process inspection[9]. In order to realize a more efficiently in-process inspection of small holes, machine vision is used in, for its simple and robust[10]. Incorporating a structured light and a charge-coupled device (CCD), the target size could be calculated by the projected image of holes on the CCD. However, this method has a drawback that a 3D object is abstracted into a 2D shadow, which neglects some fine structures.

In this paper, we developed a noncontact 3D measurement method on in-process precision hole-structure

* This work has been supported by the National Natural Science Foundation of China (Nos.11774095, 11804099 and 11621404), and the Shanghai Basic Research Project (No.18JC1412200).

** E-mail: xlchen@phy.ecnu.edu.cn

inspection based on laser triangulation and interferometers, and the point cloud data was fitted based on random sample consensus (RANSAC)[11]. Laser triangulation has a widespread application in industrial field of surface roughness test, profile measurement, and reverse engineering[12-15].

The experimental setup is illustrated in Fig.1. A CMM (ML-121510, Xian High-tech Aeh Industrial Metrology Company) was the basis of the system with the range of 1.5 m×1.2 m×1.0 m. A triangulation laser displacement sensor (ILD2300-10, Micro-Epsilon Corporation) and three home-made Michelson interferometers were fixed on the CMM, to measure the distance of the target and the displacement of the three arms of the CMM, respectively. The triangulation laser displacement sensor was suspended at the bottom of the *z*-axis mechanical arm of the CMM so that it could follow the motion of the mechanical arm. The sensor was operated based on laser triangulation method. The reflected light spot fell onto different positions of the receiving element as the target distance varied. The accuracy of the laser displacement sensor was 2 μm with the range of 10 mm. A 780-nm external cavity solid state laser (New Focus Model 6013) was coupled into a single-mode fiber. Then, the laser was splitting into 3 parts, and guided to three Michelson interferometers which were fixed on three mechanical arms. The interference signal was collected with a data acquisition card (NI USB-6356), and the displacements of three arms was calculated by a computer in real time. The interferometers have an accuracy of ~0.6 μm within a range of ~0.6 m in the experiment. Three Michelson interferometers were able to provide 3D movement data of the CMM and the laser displacement sensor could output relative displacement in one dimension. The system was calibrated by an interferometer (Chotest, SJ6000), whose accuracy was 100 nm in a range of 2 m. After calibration, the 1D displacement value was converted into 3D coordinates. In this way, this system realized 3D profile scanning of sophisticated features.

When the scanning object moved, the reflected beam spot located at different parts of the CCD target. Thus, by analyzing the movement of spot on the CCD target, the relative distance of the object could be calculated.

In the experiment, a sample of a round hole was 3D scanned. The hole was laser drilled on the surface of an aluminum alloy sheet, which was 1.4 mm thick, as shown in Fig.2. The circular hole had a diameter of ~ 0.6 mm. In the enlarged view, the edge seemed to be an ellipse, because the hole was not perpendicular to the surface and the oblique cut of cylinder was an ellipse. The scanning area was about 3.0 mm×2.5 mm, with a data rate of 100 Hz. The 3D scanning plot was obtained as shown in Fig.3(a), and 1 652 data points were obtained, which had 16 rows with an interval of about 0.15 mm. Fig.3(b) presents a specific view of 3D points cloud, which shows a series of deviation values in the hole area.

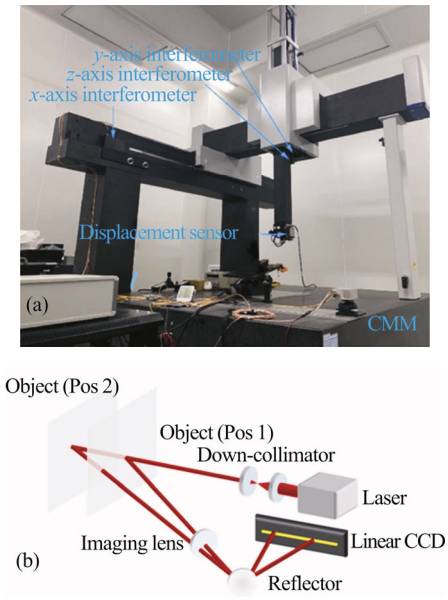

Fig.1 (a) Noncontact 3D scanning system; (b) Optical path schematic of the laser triangulation displacement sensor

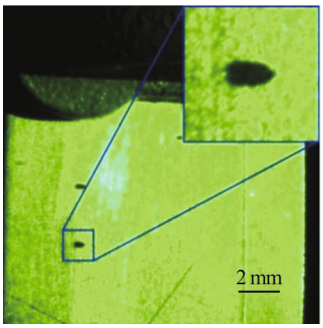

Fig.2 The picture of the object, which was illuminated by a parallel beam of green laser (The scale bar was introduced for the original figure before zoom in.)

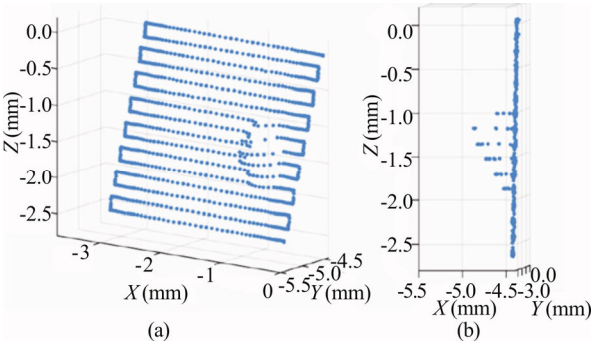

Fig.3 Raw 3D point cloud scatter plot: (a) 45° view; (b) Side view, whose direction is parallel to the surface plane

Data categorization of the 3D point cloud data was indispensable in order to calculate the parameter of the hole. Direct fitting method, such as the least squares (LS) method, appears incapable on the condition of complicated morphology and boundary. There were vast discrepancies on 3D data distributions between the surface

plane and the inner wall of the hole. Therefore, an extraction operation on 3D data of hole was proposed by using the RANSAC method. The RANSAC algorithm is widely used in machine vision, and has the prominent potential to discern varies features from raw data. The following steps describe RANSAC algorithm in detail:

(1) Randomly choose the minimum number of points from the raw data and determine the model.

(2) Calculate the residual against the model, on each point except the chosen data in step (1).

(3) Record the number n of residuals within a predefined tolerance ε.

(4) Repeat step (1) to step (4).

(5) The optimal solution is corresponding to the model which has the largest number of residuals within the tolerance ε.

In Fig.3(a), hole data points almost located around hole wall. The round hole could be abstracted to a cylinder. Fig.4 demonstrates the geometric features of a cylinder. The line through the cylinder is the axial direction of the cylinder. Point P is a point over cylindrical wall. Point P_0 is a point on the axial direction of the cylinder. The vector $\boldsymbol{u}$=(l, m, n) indicates the direction of cylindrical axis P_0N. r is the radius of the cylinder. Vector $\boldsymbol{v}$ is the normal vector of the plane. Vector $\boldsymbol{u}$ is the direction vector of the cylinder axial direction. α is the angle between $\boldsymbol{u}$ and $\boldsymbol{v}$.

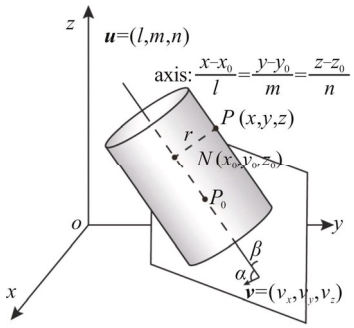

Fig.4 Cylinder and plane demonstration

Ideally, radius r equals to the distance PN from the point P on the cylindrical wall to the cylinder axial direction. Thus

$$(x-x_0)^2+(y-y_0)^2+(z-z_0)^2-\frac{\left[l(x-x_0)+m(y-y_0)+n(z-z_0)\right]^2}{l^2+m^2+n^2}=r^2. \quad (1)$$

There is always error in measuring inevitably. For each point on the cylindrical wall, the radius error equals to the difference between radius and distance from the point to cylinder axial direction. The loss equation is

$$f=\left((x-x_0)^2+(y-y_0)^2+(z-z_0)^2-\frac{\left[l(x-x_0)+m(y-y_0)+n(z-z_0)\right]^2}{l^2+m^2+n^2}\right)^{\frac{1}{2}}-r. \quad (2)$$

Let

$$h=\left((x-x_0)^2+(y-y_0)^2+(z-z_0)^2-\frac{\left[l(x-x_0)+m(y-y_0)+n(z-z_0)\right]^2}{l^2+m^2+n^2}\right)^{\frac{1}{2}}. \quad (3)$$

Eq.(2) could be expressed as

$$f(x_0, y_0, z_0, l, m, n, r)=h(x_0, y_0, z_0, l, m, n)-r. \quad (4)$$

According to LS principle[16,17], when the sum of error square gets minimized, the optimal parameters is

$$\hat{\theta}=\arg\min\sum_{i=1}^{n}(h_i-r)^2. \quad (5)$$

The radius r and axial direction (l, m, n) of the hole could be calculated by Eq.(5). According to geometrical relationship, the angle between the cylinder axial direction and normal direction of the surface plane is

$$\alpha=\arccos\frac{\boldsymbol{u}\cdot\boldsymbol{v}}{|\boldsymbol{u}|\cdot|\boldsymbol{v}|}. \quad (6)$$

Industrially, the needs of hole inspection were widespread. To evaluate the method mentioned above, we used traditional projection method to measure the diameter and angle of the hole[18]. Illuminated by a large-beam collimator (520 nm, 100 mm in diameter, 0.01 mrad of the divergence angle), the metal sheet was fixed on a rotary table, and rotated in two-dimensional. For each step of rotation, the rotary table rotated 1°, with an accuracy of 0.05°. A CCD camera took pictures while the sample was rotated to each angle. The hole contour had a largest projection on the target, while it was perpendicular to the optical axis of the CCD camera. Canny edge operator was used to detect the boundary[19], after converting the pictures into grayscale images. The hole contour was an ellipse, so the major axis and minor axis of ellipse of each image were calculated by ellipse fitting[16]. Due to its geometric projective characteristics, the minor axis could be considered as the cylinder diameter. Fig.5 shows nine grayscale images from different directions. The rotary table has two rotational degrees of freedom, azimuth and tilt. For each rotation, the rotary table rotates 1° in one direction. The middle subplot in this figure represents the largest projection of the hole contour, and its direction is marked as 0° azimuth and 0° tilt. Red curves were the fitting ellipses. The middle ellipse had the largest size. A smooth elliptic curve was obtained by the edge recognition method. The diameter was estimated to 620.228 μm. The precision of edge recognition depended on several factors: surface roughness of the target, laser beam parallelism and pixel size.

In the same way, a plug gauge (600 μm in diameter with an accuracy of 1 μm) was plug into the hole[18]. Fixed horizontally on the rotary table, the sample would rotate horizontally, as shown in Fig.6. The CCD camera took pictures after each rotation. OA was the plug gauge. OB was the projection of OA onto the metal plane. $\angle AOB$ was the angle between the hole and the plane surface, thus the inclined angle equals to the complementary angle of $\angle AOB$. When plane AOB was parallel to the optical axis of the CCD camera, $\angle AOB$ got the minimum value. Collecting a series of images, the angles

between the plug gauge and the plane were calculated. The estimated angle was 56.122 2°.

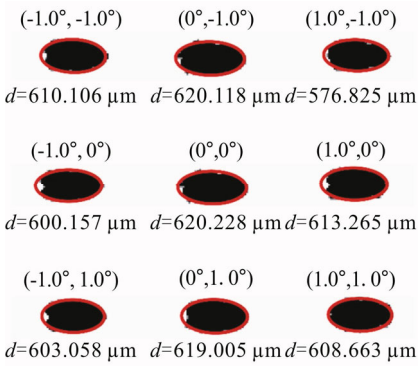

Fig.5 Binary images of the hole from nine directions

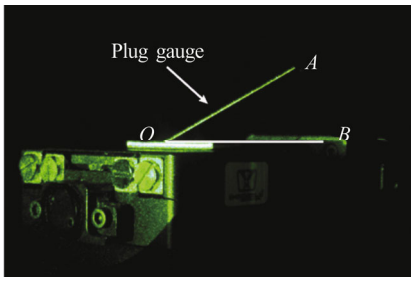

Fig.6 Experimental setup image of the hole inclined angle measurement

Using RANSAC method, the raw 3D data was classified to two parts of the surface plane and the inner wall of the hole, respectively. Fig.7 shows the categorization of 3D data points using RANSAC operation. In Fig.7(a), the elliptical vacant area of the scatter plot was the contour section of the round hole. Fig.7(b) presents the 3D data points of the inner wall of the hole, which mainly distribute around a partial cylindrical wall. For the 3D data of the surface plane, the linear regression process[16,17] was used. The calculation of the normal vector $\boldsymbol{v}$ of the surface plane was (0.046 7, 0.998 8, −0.016 8).

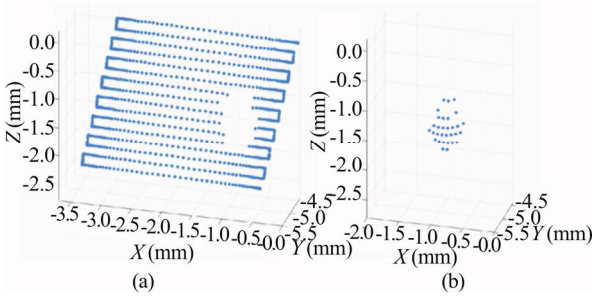

Fig.7 Extracted data after RANSAC operation: (a) Plane data; (b) Hole data

In Fig.7(b), there was 31 data points of the hole distilled from raw data. As the displacement sensor could not rotate freely and it just measure towards a single direction, only partial cylindrical hole could be scanned. Excessive point concentration from a local area may lead to calculation error. However, the contour of the cylinder was visually and the computing result was satisfactory, due to the proper scanning intervals. The cylinder axial direction was calculated as (−0.034 8, −0.328 8, 0.506 1), and the diameter of the hole was 648.609 μm after LS fitting. According to Eq.(6), the inclined angle between the hole axial direction and plane was 55.945 9°. Most points of the hole located at the cylindrical wall regularly. However, several points around the contour of the hole distributed dispersively. This phenomenon originated from the deformation of spot on the hole contour, in which a part of the spot located on the surface, and the other part was in the hole. Thus, they became the measurement errors, which would be reduced by a smaller spot size. In order to reconstruct an ideal cylinder, the points with distance from the surface within 100 μm were filtered. The error derived by the contour would decrease and the spot distortion on the hole wall would be reduced, while the spot size had become smaller. The fitting parameters calculated by the 3D scanning method and the projection method are shown in Tab.1. The diameter error was about 28.4 μm and the inclined angle error was less than 0.2°. The laser displacement sensor employed centroid method to determine spot location, so it was high-demanding in laser spot quality. The measurement accuracy deteriorates greatly, because the reflected spot was deformed and misshaped from the bending of morphology in the hole and block by the hole wall.

Tab.1 Measurement results

Method	Diameter (μm)	Angle (°)
3D scanning	648.609	55.946
Projection method	620.228	56.122

In conclusion, a noncontact measuring system and data process method are proposed for the purpose of precise optical measurement of hole structure. Its validity and reliability were verified in the experiment. The CMM's probe used a laser displacement sensor and the location data are supplied by three home-made Michelson interferometers. The RANSAC approach was used to extract the 3D data of the inner wall of the hole from the raw data. After data cleaning and filtering, the LS optimization method was employed to calculate the diameter and the angle of the hole. The result was compared with data measured with a plug gauge, by projection method. The estimated error of the diameter and the angle in these two methods were less than 30 μm and 0.2°, respectively. In the next research, a rotating mechanical structure of the laser displacement sensor would be installed, so that this scanning system could scan the full view of the hole internally, rather than partial hole. In this approach, more data would be generated and the estimation can fit the characteristics better. The 3D scanning method presented the advantages of noncontact measurement, high precision, high speed, reliable algorithm and the ability of tiny

structure scanning, which meets the requirement of machinery industry and expresses practicality in manufacturing.

References

[1] Wu Qing-yang, Zhang Bai-chun, Lin Hai-xin and Zeng Xiang-jun, Chinese Optics Letter **14**, 010010 (2016).

[2] Bian Xing-yuan, Cui Jun-ning and Lu Ye-sheng, Applied Sciences **9**, 242 (2019).

[3] Usman Z., Monfared R. P., Lohse N. and MR Jackson, International Journal of Metrology and Quality Engineering **7**, 2 (2016).

[4] S. Marimuthu, M. Antar and J. Dunleavey, Precision Engineering **55**, 339 (2019).

[5] Peiner E. and Doering L., IEEE Sensors Journal **13**, 2 (2012).

[6] Bi Chao, Fang Jian-guo, Li Kun and Guo Zhi-jun, Chinese Journal of Aeronautics **30**, 4 (2017).

[7] Gao Xin-xing, Zhao Bin and Wang Qi-wei, Review of Scientific Instruments **90**, 9 (2019).

[8] Su Zhi-qi, He Qing and Xie Zhi, Review of Scientific Instruments **87**, 3 (2016).

[9] Kao Chen-chun and Albert J. Shih, Measurement Science and Technology **18**, 11 (2007).

[10] Yu Long, Bi Qing-zhen, Ji Yu-lei, Fan Yun-fei, Huang Nuo-di and Wang Yu-han, Precision Engineering **58**, 35 (2019).

[11] Fischler Martin A. and Robert C. Bolles, The IEEE International Conference on Computer Vision (ICCV), 4332 (2019).

[12] Simone Donadello, Maurizio Motta, Ali Gokhan and Barbara Previtali, Optics and Laser in Engineering **112**, 136 (2019).

[13] Zhang Xiao-bo, Fan Fu-min, Mehdi Gheisari and Gautam Srivastava, IEEE Access **7**, 64837 (2019).

[14] Gerardo Antonio, Jose Mauricio and Renato Coral, Sensors **19**, 8 (2019).

[15] Johannes Schlarp, Ernst Csencsics and Georg Schitter, IEEE Transactions on Instrumentation and Measurement **69**, 6 (2019).

[16] Wang Kang-wei, Zhang Xin, Hao Qiu-shi, Wang Yan and Shen Yi, Neurocomputing **332**, 7 (2019)

[17] Rana Muhammad, Liang Zhong-min, Salim Heddam, Mohammad Zounemat-Kermani, Ozgur Kisi and Binquan Li, Journal of Hydrology **586**, 124371 (2020).

[18] Amir Novini, Optics, Illumination, and Image Sensing for Machine Vision **728**, 84 (1987).

[19] D. Sangeetha and P. Deepa, Journal of Real-Time Image Processing **16**, 957 (2019).